Separation of presynaptic Ca_V2 and Ca_V1 channel function in synaptic vesicle exo- and endocytosis by the membrane anchored Ca^{2+} pump PMCA

Niklas Krick[a], Stefanie Ryglewski[a], Aylin Pichler[a], Arthur Bikbaev[a], Torsten Götz[b], Oliver Kobler[c], Martin Heine[a], Ulrich Thomas[d,1], and Carsten Duch[a,1]

[a]Institute of Developmental Biology and Neurobiology, Johannes Gutenberg University Mainz, 55128 Mainz, Germany; [b]Institute for Biology/Genetics, Freie Universität Berlin, 14195 Berlin, Germany; [c]Combinatorial NeuroImaging Core Facility, Leibniz Institute for Neurobiology, 39118 Magdeburg, Germany; and [d]Department of Neurochemistry and Molecular Biology, Leibniz Institute for Neurobiology, 39118 Magdeburg, Germany

Edited by John G. Hildebrand, The University of Arizona, Tucson, AZ, and approved June 4, 2021 (received for review April 15, 2021)

Synaptic vesicle (SV) release, recycling, and plastic changes of release probability co-occur side by side within nerve terminals and rely on local Ca^{2+} signals with different temporal and spatial profiles. The mechanisms that guarantee separate regulation of these vital presynaptic functions during action potential (AP)–triggered presynaptic Ca^{2+} entry remain unclear. Combining *Drosophila* genetics with electrophysiology and imaging reveals the localization of two different voltage-gated calcium channels at the presynaptic terminals of glutamatergic neuromuscular synapses (the *Drosophila* Ca_V2 homolog, Dmca1A or cacophony, and the Ca_V1 homolog, Dmca1D) but with spatial and functional separation. Ca_V2 within active zones is required for AP-triggered neurotransmitter release. By contrast, Ca_V1 localizes predominantly around active zones and contributes substantially to AP-evoked Ca^{2+} influx but has a small impact on release. Instead, L-type calcium currents through Ca_V1 fine-tune short-term plasticity and facilitate SV recycling. Separate control of SV exo- and endocytosis by AP-triggered presynaptic Ca^{2+} influx through different channels demands efficient measures to protect the neurotransmitter release machinery against Ca_V1-mediated Ca^{2+} influx. We show that the plasma membrane Ca^{2+} ATPase (PMCA) resides in between active zones and isolates Ca_V2-triggered release from Ca_V1-mediated dynamic regulation of recycling and short-term plasticity, two processes which Ca_V2 may also contribute to. As L-type Ca_V1 channels also localize next to PQ-type Ca_V2 channels within axon terminals of some central mammalian synapses, we propose that Ca_V2, Ca_V1, and PMCA act as a conserved functional triad that enables separate control of SV release and recycling rates in presynaptic terminals.

synapse | *Drosophila* | Dmca1D | cacophony | PMCA

Neuronal network function critically depends on the tight control of synaptic vesicle (SV) release probability at chemical synapses over wide ranges of activity regimes. At the same time, synaptic gain remains adjustable to render network function flexible. To maintain synapse function over time, SV recycling rates must be matched to vastly different activity patterns and synaptic gains. While SV release and recycling as well as their plasticity-related adjustments all include Ca^{2+}-dependent steps, they operate in parallel but on different time scales. A tight spatial and temporal coordination of presynaptic Ca^{2+} signals and their effectors is thus needed for both the induction of changes in synaptic strength and the maintenance of robust synapse function. However, the mechanisms that effectively separate Ca^{2+} signals in time and space (e.g., through different voltage-gated calcium channels [VGCCs]) to allocate these to different presynaptic functions are not well understood.

SV release probability depends on the sensitivity of the vesicular Ca^{2+} sensor and the positioning of VGCCs inside active zones (AZs) (1). Various mechanisms that can tune release probability by modulating their precise localization or kinetic properties have been uncovered (2–4). Irrespective of such modulation, efficient Ca^{2+}-triggered SV release through presynaptic VGCCs (mainly $Ca_V2.1$ and $Ca_V2.2$ in vertebrates) remains spatially restricted to a few hundred nanometers due to the limited abundance and brief opening of the channels and the presence of endogenous Ca^{2+} buffers (5, 6). It is thus conceivable that Ca^{2+} signals originating within presynaptic terminals but outside AZs are engaged to tune SV recycling and plastic changes according to changes in activity.

Apart from the need for fast activating and inactivating Ca_V2 channels for SV release, other types of VGCCs have been implicated in presynaptic plasticity. In GABAergic synapses, pharmacological blockade of Ca_V1 channels does not affect AP-induced SV release but converts posttetanic potentiation into synaptic depression (7). In hippocampal CA3 mossy fiber boutons (8–10) or in synapses of the lateral amygdala (11), $Ca_V2.3$ and $Ca_V1.2$ channels are required for presynaptic long-term plasticity but are unable to trigger SV release (9, 11).

Differential functions of Ca_V2 and Ca_V1 channels in neurotransmitter release versus other Ca^{2+}-dependent presynaptic processes can hardly be explained just by different coupling distances to SVs, since there are also situations where loose coupling is predominant (4, 10). Moreover, compared with

Significance

Synaptic vesicle (SV) release from presynaptic terminals requires nanometer precise control of action potential (AP)–triggered calcium influx through voltage-gated calcium channels (VGCCs). SV recycling also depends on calcium signals, though in different spatiotemporal domains. Mechanisms for separate control of SV release and recycling by AP-triggered calcium influx remain elusive. Here, we demonstrate largely independent regulation of release and recycling by two different populations of VGCCs (Ca_V2, Ca_V1), identify Ca_V1 as one of potentially multiple calcium entry routes for endocytosis regulation, and show functional separation of simultaneous calcium signals in the nanometer space of a presynaptic terminal by the plasma membrane calcium ATPase (PMCA). The Ca_V2/Ca_V1/PMCA functional triad may provide conserved means for independent control of different vital presynaptic functions.

Author contributions: N.K., M.H., U.T., and C.D. designed research; N.K., S.R., A.P., T.G., O.K., M.H., U.T., and C.D. performed research; A.B. and O.K. contributed new reagents/analytic tools; N.K., S.R., A.P., A.B., O.K., M.H., U.T., and C.D. analyzed data; and N.K., U.T., and C.D. wrote the paper.

The authors declare no competing interest.

This article is a PNAS Direct Submission.

[1]To whom correspondence may be addressed. Email: cduch@uni-mainz.de or Ulrich.Thomas@lin-magdeburg.de.

This article contains supporting information online at https://www.pnas.org/lookup/suppl/doi:10.1073/pnas.2106621118/-/DCSupplemental.

Published July 8, 2021.

$Ca_v2.1$ and $Ca_v2.2$, Ca_v1 channels display higher conductances (12), suggesting that additional mechanisms are required to allocate Ca_V1-related Ca^{2+} signals to specific presynaptic functions while avoiding interference with SV release. SV recycling also includes regulation by presynaptic Ca^{2+} signals but operates mostly at different subsynaptic sites and at slower time scales than Ca^{2+}-triggered SV release (13–15). We hypothesize that activity-dependent regulation of SV recycling employs Ca_v1-dependent Ca^{2+} entry and that active mechanisms exist to regulate the relative contributions of Ca_v2 and Ca_v1 channels to SV release versus recycling. We address these hypotheses at the *Drosophila* larval neuromuscular junction (NMJ), an established model for glutamatergic synapse function (16–18).

Results

AP-Triggered Presynaptic Ca^{2+} Influx through Spatially Separated Ca_v2 and Ca_v1 Channels. AP-induced neurotransmitter release at the NMJ depends on close proximity of Ca_v2 channels to readily releasable SVs in AZs established by interactions with the cytomatrix protein Bruchpilot (Brp) (17). While confirming the colocalization of Brp and the *Drosophila* Ca_v2 homolog, Dmca1A (cacophony), at presynaptic AZs (Fig. 1*A*), we newly identified the localization of the Ca_v1 channel homolog, Dmca1D, in presynaptic axon terminals (Fig. 1*B*). Antibody specificity has previously been demonstrated by Western blotting and selective labeling of control neurons in Ca_v1 null mosaic mutants (19). Quantitative image analysis yielded a Pearson correlation coefficient (PCC) of 0.655 ± 0.028 SD ($n = 8$) for Ca_v2/Brp (*SI Appendix*, Fig. S1 *A* and *C*). The Mander's coefficients (M1, M2) indicated that by far most of the Brp label is positive for Ca_v2 (M2 = 0.842 ± 0.042 SD), whereas ∼40% of the Ca_v2 label remains negative for Brp (M1 = 0.608 ± 0.066 SD, *SI Appendix*, Fig. S1*D*). By contrast, Ca_v1 localizes predominantly outside Brp-labeled AZs (Fig. 1*B*), although some Ca_v1 label also reaches into AZs (Fig. 1*B*, white arrows). Specifically, the PCC for Brp/Ca_v1 is 0.297 ± 0.027 SD ($n = 10$) and >70% of the Ca_v1 label remains Brp negative (M1 = 0.275 ± 0.032 SD), whereas ∼60% of the Brp label displays co-occurrence of Ca_v1 (M2 = 0.611 ± 0.034, *SI Appendix*, Fig. S1 *B–D*).

Differential localization of Ca_v2 and Ca_v1 channels in and around AZs have also been described in hippocampal neurons (20), but the functional implications of this organization remain unknown. Both chronic and acute manipulation of Ca_v1 reveal a significant contribution to AP-triggered net presynaptic Ca^{2+} influx at the NMJ. Targeted RNAi knockdown of Ca_v1 (Ca_v1-kd) reduces AP-induced net Ca^{2+} influx into the presynaptic terminal by ∼50% (Fig. 1 *C–F*). Ca_v1-kd did not cause changes in synaptic structure, arguing against developmental effects (*SI Appendix*, Fig. S2 *A–F, i*). Moreover, acute reduction of Ca_v1 currents by bath application of the endogenous neuromodulator tyramine (21) reversibly reduces evoked presynaptic Ca^{2+} influx in controls but not after Ca_v1-kd (Fig. 1 *G* and *H*).

Ca_v2 but not Ca_v1 Channels Are Required for Evoked SV Release. We next analyzed the contribution of either presynaptic high voltage-activated (HVA) calcium channel to synaptic transmission. Although the reduction of Ca_v1 by bath application of tyramine significantly reduces AP-triggered presynaptic Ca^{2+} influx (Fig. 1 *G* and *H*), it has no obvious effect on evoked synaptic transmission (Fig. 1*I*). Chronic Ca_v1-kd in motoneurons has only minor effects on evoked postsynaptic potentials (PSPs) (Fig. 1*J*), but it causes a reduction in the amplitude of evoked postsynaptic currents (PSCs) by 10 to 20% that is statistically significant at 0.5 mM (Figs. 1 *K* and *L*) but not at 2 mM external Ca^{2+} (*SI Appendix*, Fig. S2 *G* and *H*). Consequently, paired pulse facilitation is significantly increased upon Ca_v1-kd (Fig. *1* K and *M*; *SI Appendix*, Fig. S2 *I* and *J*). Hence, the small impact that Ca^{2+} influx through Ca_v1 exerts on SV release triggered by a single AP has consequences on short-term plasticity. By contrast, acute loss of Ca_v2 channel function in temperature-sensitive mutants nearly eliminates synaptic transmission (Fig. 1*N*), and mutants are paralyzed at nonpermissive temperature (22). Temperature shifts per se also reduce synaptic transmission in controls (Fig. 1*N*), but PSPs can still be evoked reliably, and control animals show muscle contractions and coordinated motor behavior at 35 °C. Similarly, employing the FlpStop technique to knock out Ca_v2 in subsets of motoneurons reduces the amplitude of PSCs by ∼90% selectively at respective synapses (Fig. 1 *O–Q*). In sum, Ca_v2 channels localize to AZs and contribute to ∼90% of evoked SV release, whereas Ca_v1 channels localize predominantly around AZs and make a small contribution to evoked release that affects short term plasticity. We next tested whether Ca_v1 channels mediate additional functions at the presynaptic terminal.

AP-Triggered Presynaptic Ca^{2+} Influx through Ca_v1 Augments SV Recycling. Separate control of SV exocytosis and endocytosis by Ca^{2+} influx through distinct routes has previously been suggested for the *Drosophila* NMJ (23) as well as for vertebrate synapses (24), but the channel identity and Ca^{2+} entry route for endocytosis regulation remain unknown. We find that Ca_v1 channels localize mainly around AZs (Fig. 1*B*), underlie slowly inactivating L-type like currents (19), and contribute significantly to AP-triggered presynaptic Ca^{2+} influx (Fig. 1 *E–H*). Therefore, Ca_v1 localization and properties are well suited for activity-dependent modulation of SV endocytosis. In line with this hypothesis, we find increased synaptic depression during sustained activity upon Ca_v1-kd, both in low (Fig. 2 *A* and *B*) and in high external Ca^{2+} (*SI Appendix*, Fig. S3 *A* and *B*). With Ca_v1-kd (Fig. 2*B*) or knockout (*SI Appendix*, Fig. S3 *C–E*), synaptic depression is increased already after 5 s, and, after 15 to 20 stimuli, a significantly reduced steady state PSC amplitude is reached (Fig. 2*B* and *SI Appendix*, Fig. S3*E*). This, however, could still reflect an involvement of Ca_v1 in multiple steps of the SV cycle. We therefore conducted additional experiments to probe our hypothesis that Ca_v1 functions in SV endocytosis regulation.

First, we tested whether endocytosis was required to see the effect of Ca_v1-kd on synaptic depression. Here, we repeated the experiments in Fig. 2 *A* and *B* under acute blockade of endocytosis with dynasore (25). This led to increased synaptic depression during 1 Hz stimulation in control, whereas there was no additional effect on depression for Ca_v1-kd (Fig. 2*C*). Moreover, the difference observed between control and Ca_v1-kd after 5 s (Fig. 2 *A* and *B*) is largely abolished with dynasore (Fig. 2*C*), and, for both Ca_v1-kd and control, PSC amplitudes decline to ∼65% of their initial amplitude within 75 s of stimulation (Fig. 2*C*). Therefore, the effect of Ca_v1-kd on synaptic depression is highly dependent on ongoing SV endocytosis, thus indicating a role of Ca_v1 in SV endocytosis regulation. A slightly faster decline of PSC amplitudes for Ca_v1-kd in between ∼10 and 30 s of stimulation (Fig. 2 *C*, *Inset*) might point to an additional fast function of Ca_v1, such as SV recruitment to release sites or priming. However, compared with the difference in synaptic depression that requires endocytosis, this effect of Ca_v1-kd is small and was not further investigated.

Second, we tested whether Ca_v1-kd altered the size of the readily releasable pool (RRP) of SVs. We estimated RRP size in control and with motoneuronal Ca_v1-kd by cumulative PSC charge analysis during brief high-frequency stimulation (1 s, 60 Hz, Fig. 2 *D–F*) in 2 mM external Ca^{2+}. Cumulative PSC charge was calculated by back-extrapolation of a linear fit from the last 15 stimuli of the cumulative PSC integrals to time point zero (Fig. 2*E*). RRP size was estimated by dividing cumulative PSC charge by the average mPSC charge (26). RRP sizes were not statistically different ($P = 0.33$, *t* test) between control (3,052 ± 281 SEM) and Ca_v1-kd (2,786 ± 360 SEM, Fig. 2*F*). Therefore, increased synaptic depression with Ca_v1-kd is unlikely a consequence of altered RRP size.

To test a potential role of Ca_v1 in SV endocytosis more directly, we employed synaptopHluorin imaging to measure SV

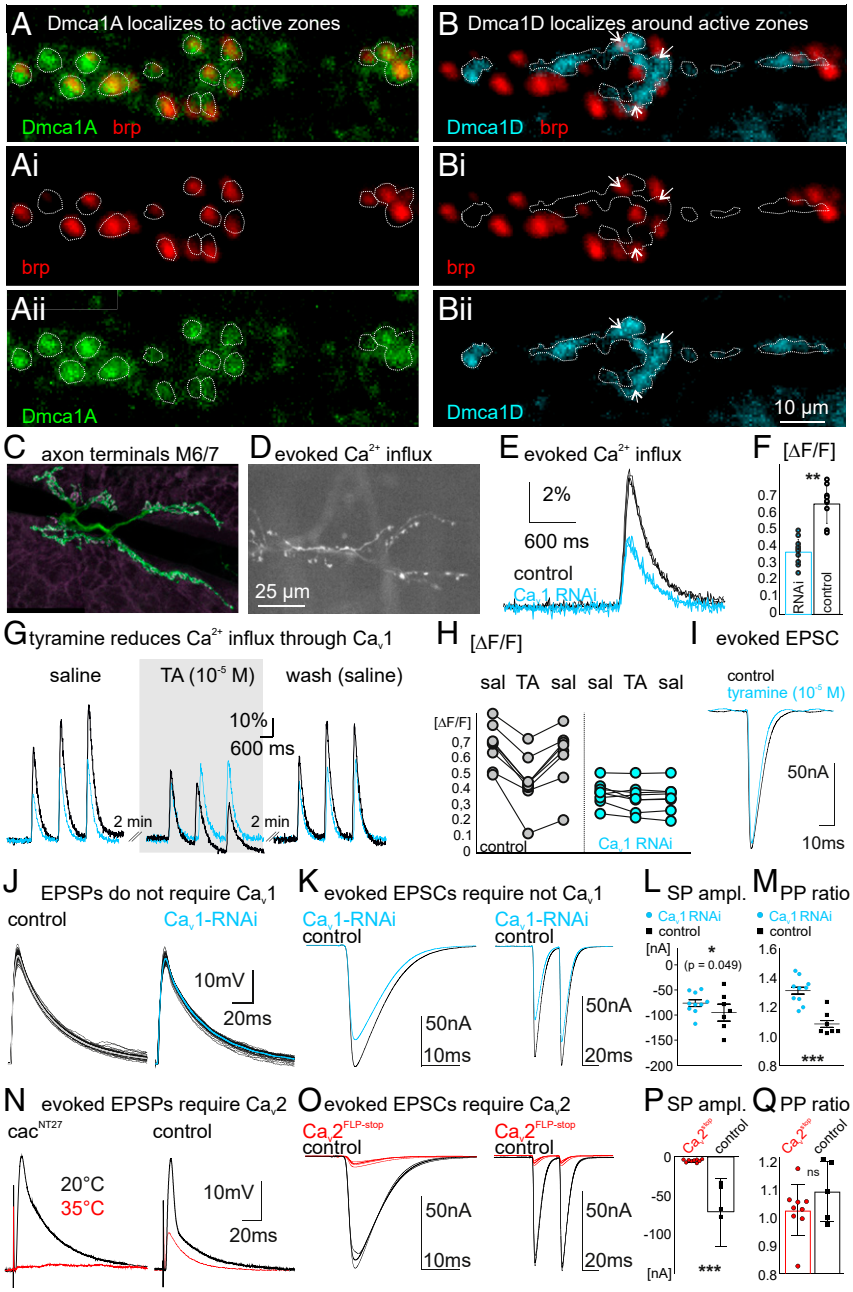

Fig. 1. Distinct localization and functional impact of Ca_v1 and Ca_v2 in presynaptic terminals. (*A* and *B*) Triple labeling for Ca_v2 channels, the AZ marker Brp, and Ca_v1 channels in type Ib boutons of muscles M6/7. Whereas Brp (red, *A*, *i*) and the Ca_v2 channel homolog, Dmca1A (green, *A*, *ii*) display colocalization at AZs (*A*), the Ca_v1 homolog Dmca1D (*B*, *ii*, blue, dotted white line) localizes mostly around AZs (*B*, *i*, red), but some Ca_v1 label overlaps with AZs (white arrows). (*C*–*F*) Representative motoneuron axonal projections (green) with AZs (magenta) on M6/7 (*C*) and with expression of GCaMP6m (*D*). (*E*) Presynaptic Ca^{2+} signals in response to trains of 10 APs at 100 Hz in controls (black traces) and following Ca_v1-kd in motoneurons. (*F*) Quantification reveals a significant reduction of net presynaptic Ca^{2+} influx upon Ca_v1-kd. (*G* and *H*) Acute reduction of Ca_v1 channel function by bath application of tyramine (10^{-5} M) reversibly reduces presynaptic Ca^{2+} responses within 2 min in controls (*G*, black traces and *H*, gray circles) but not upon Ca_v1-kd (*G*, blue traces; *H*, blue circles). (*I*) Bath application of tyramine has no obvious effect on evoked PSCs. (*J*) Evoked PSPs recorded in current clamp mode from M6/7 in control (*Left*, overlay of 20 consecutive PSP traces, average in gray) and with motoneuronal Ca_v1-kd (*Right*, overlay of 20 consecutive PSP traces, average in blue) indicate no differences. (*K*–*M*) Responses to single and paired stimuli. Evoked PSCs recorded in voltage clamp mode from M6/7 (*K*) in controls (*Left*, black trace) and with motoneuronal Ca_v1-kd (*Left*, blue trace) reveal a small but statistically significant ($P = 0.049$, Student's *t* test) reduction in PSC amplitude upon Ca_v1-kd (*L*). Paired pulse facilitation (*K*, control, black trace, Ca_v1 RNAi, blue trace) is significantly increased upon Ca_v1-kd (M). (*N*) In temperature-sensitive Ca_v2 mutants (cac^{NT27}, *Left* traces), PSPs recorded from M6/7 are normal at 20 °C (black trace) but nearly eliminated at nonpermissive temperature (35 °C, red trace). In controls (*Right* traces), PSPs are reduced at 35 °C but not eliminated. (*O*–*Q*) In mosaic Ca_v2 null mutants generated with the FLP-stop method, PSC amplitude is reduced by >90% at Ca_v2 knock out synapses (red traces) but normal at control NMJs (black traces). (*P*) Quantification of single pulse (SP) amplitudes and paired pulse ratios (*Q*) in Cav2 null versus control synapses. $*P < 0.05$; $**P < 0.01$; $***P < 0.001$; ns, not significant.

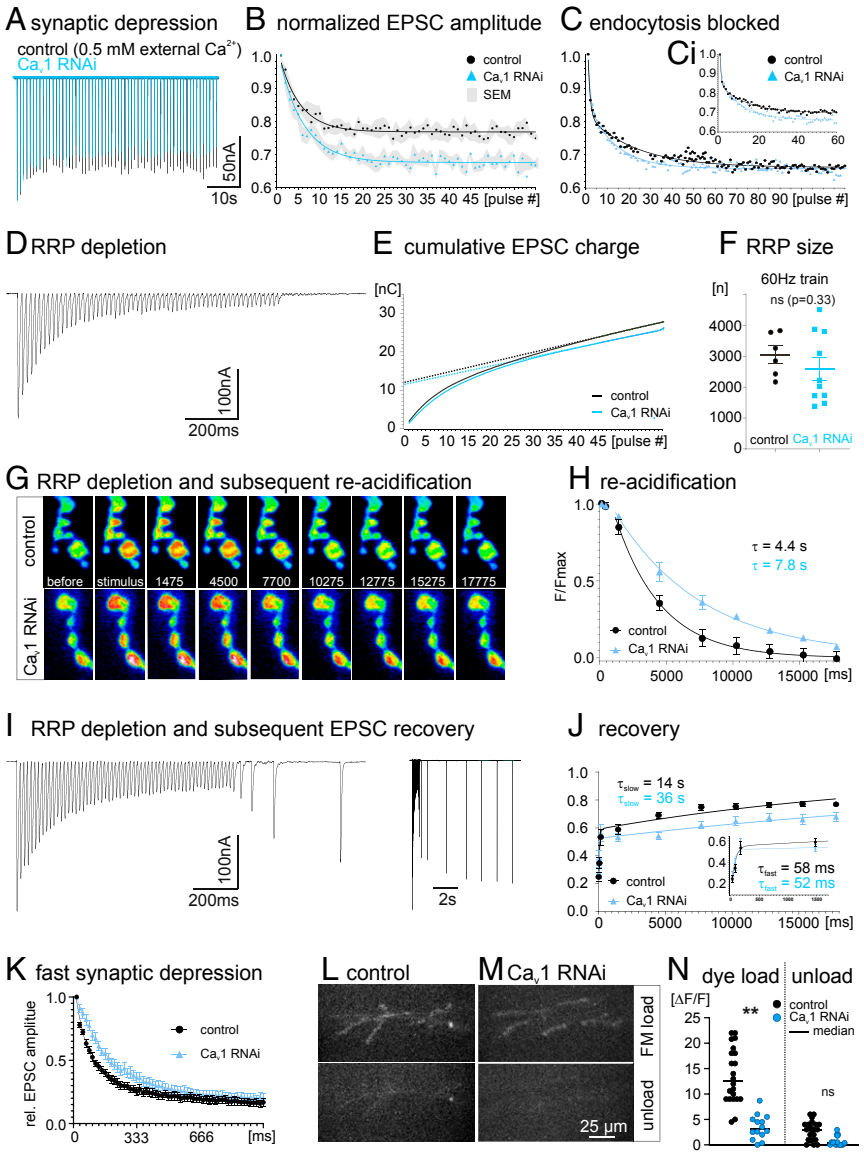

Fig. 2. Activity dependent Ca^{2+} influx through presynaptic Ca_v1 augments SV recycling. (*A*) Representative recordings of PSCs from muscle M6/7 during 1 min of motoneuron stimulation at 1 Hz in control (black trace) and following Ca_v1 RNAi in motoneurons (blue trace) indicate increased synaptic depression with Ca_v1 RNAi. (*B*) For quantification, PSC amplitude was normalized to the first PSC and averaged over 6 control (black circles) and 6 motoneuronal Ca_v1-kd animals (blue triangles). Lines indicate single exponential fits, and gray shaded areas represent the SEM. Steady-state synaptic depression is reached after ~25 stimuli and increased by 45% upon Ca_v1-kd. (*C*) Similar experiment as in *B* but with endocytosis blocked by dynasore (80 µM). Normalized PSC amplitudes during 1 Hz motoneuron stimulation for 2 min in control (black trace) and following Ca_v1 RNAi decline to identical values of steady-state synaptic depression. The time course of PSC amplitude decline is faster within Ca_v1-kd (see inset *Ci*). (*D*) Representation EPSC trains in response to a stimulus train of 1 s duration at 60 Hz (2 mM [Ca^{2+}]). Cumulative EPSC charge was calculated for control (black line) and Ca_v1-kd by back-extrapolation of a linear fit (dotted lines) to the last 15 stimuli of the cumulative EPSC integrals to time point zero. (*F*) RRP size was estimated by dividing cumulative EPSC charge by the average mEPSC charge for control (black circles) and Ca_v1-kd (blue squares). Mean values are indicated by horizontal bars and SD by error bar. (*G*) Representative false color-coded snapshots of synaptopHluorin imaging from boutons on M6/7 before, during, and at different time intervals after RRP depletion with a 1 s train of 60 Hz stimulation (upper row control, $n = 35$ boutons from 7 animals, lower row Ca_v1 kd, $n = 30$ boutons from 6 animals). (*H*) Quantification as ΔF/F at increasing time intervals shows significantly reduced SV recycling with Ca_v1 kd (blue) compared with the control (black). Between the 1,475 and 17,775 ms intervals, fluorescence decline is fitted with single exponentials (lines). Time constant of decay is significantly increased by Ca_v1 kd from 4.4 to 7.8 s. (*I*) Representative PSCs during RRP depletion induced by 60 Hz stimulation train for 1 s, followed by single evoked responses at 11 different time points after the train (at 25, 75, 175, 475, 1,475, 4,500, 7,700, 10,275, 12,275, 15,275, and 17,775 ms). Train and first 5 PSCs after RRP depletion (*Left*) and whole trace (*Right*). (*J*) Normalized average recovery PSC amplitudes at different posttrain time points divided by first PSC amplitude of the train for control (black circles, $n = 8$) and Ca_v1 RNAi (blue triangles, $n = 7$). Data are fitted biexponentially (lines). Ca_v1 kd does not affect the fast recovery component significantly but significantly increases the time constant of the slow recovery component from 14 to 36 s. (*K*) PSC amplitudes during 60 Hz stimulation for 1 s normalized to the first PSC amplitude of the train show similar amounts of synaptic depression at the end of the stimulation train in control (black) and with Ca_v1 kd. (*L–N*) *Upper* panels (FM load) show representative images of FM1-43 dye taken up into recycled SVs in axon terminals on M6/7 after stimulation with high K^+ (20 mM) for 3 min followed by 3 min wash in Ca^{2+} free saline in a control (*Left*) and with Ca_v1-kd (*Right*). Restimulation for 5 min in high K^+ causes nearly complete unloading of labeled SVs (*Lower* panels) in control (*Left*) and with Ca_v1-kd (*Right*). (*N*) Quantification reveals significantly reduced dye load with Ca_v1-kd (blue circles) compared with the control (black circles). By contrast, activity-induced SV release (unload) is not significantly affected. $^{**}P < 0.01$; ns, not significant.

acidification after RRP depletion with high-frequency stimulation (1 s train at 60 Hz; Fig. 2 *G* and *H*). In both control and Ca_v1-kd, SV release during the stimulus train caused synaptopHluorin fluorescence increases (Fig. 2 *G*, *Left*), followed by fluorescence decreases due to SV recycling and acidification, which was measured at 8 different time points (between 175 and 17,775 ms after stimulation with increasing time intervals between measurements). With Ca_v1-kd, the time course of SV acidification was significantly slower ($\tau = 7.8 \pm 1.1$ s, $n = 6$) compared with the control ($\tau = 4.4 \pm 1.1$ s, $n = 7$; $P < 0.01$, *t* test). A significant difference with Ca_v1-kd was observed already ~5 s after the stimulation train, thus matching the timing of the effect of Ca_v1-kd on synaptic depression during low-frequency stimulation (Fig. 2 *A* and *B*). These data lend further support to a role of Ca_v1 in augmenting SV endocytosis.

To compare the time courses of SV acidification and PSC amplitude recovery after presynaptic RRP depletion, we measured PSC amplitude at the same 8 time points after stimulation trains of 1 s duration and 60 Hz frequency (Fig. 2 *I* and *J*). The stimulation train caused synaptic depression by ~80% in control and Ca_v1-kd condition (Fig. 2*K*). Following RRP depletion, PSC amplitude recovery follows a fast and a substantially slower time course (26). The fast recovery time constant of ~50 ms was not significantly affected by Ca_v1-kd (Fig. 2*J*). By contrast, the slow recovery time constant was significantly increased by Ca_v1-kd (36.6 s) compared with the control (14.5 s). Finally, a role of Ca_v1 in SV endocytosis is also supported by imaging the uptake and release of the styryl dye FM1-43. Following bath application of high K^+ (20 mM) for 3 min, FM1-43 uptake into recycled SVs was significantly reduced by Ca_v1-kd (Fig. 2 *L*–*N*). By contrast, unloading of labeled SVs by reactivating synaptic transmission in high K^+ was not affected (Fig. 2 *L*–*N*).

Together, these data indicate that activity-dependent Ca^{2+} influx through Ca_v1 facilitates SV recycling. However, Ca_v1-kd does not eliminate PSC amplitude or synaptopHluorin signal recovery after RRP depletion but slows the recovery time constant. Therefore, Ca^{2+} entry through Ca_v1 is not mandatory for SV endocytosis, but it has an augmenting effect. Moreover, the effects of Ca_v1-kd on synaptic depression (Fig. 2 *A* and *B*), synaptopHluorin signal (Fig. 2 *G* and *H*), and PSC amplitude recovery (Fig. 2 *I* and *J*) manifest within 5 s. Full membrane recycling, new SV formation, and vesicle filling is difficult to reconcile with this speed, unless ultrafast recycling and very fast SV reformation take place. It has been demonstrated, however, that endocytic proteins can also function in release site clearance (27). Therefore, reduced endocytosis in Ca_v1-kd could potentially increase synaptic depression or slow recovery from RRP depletion by reducing the speed of release site clearance. Either

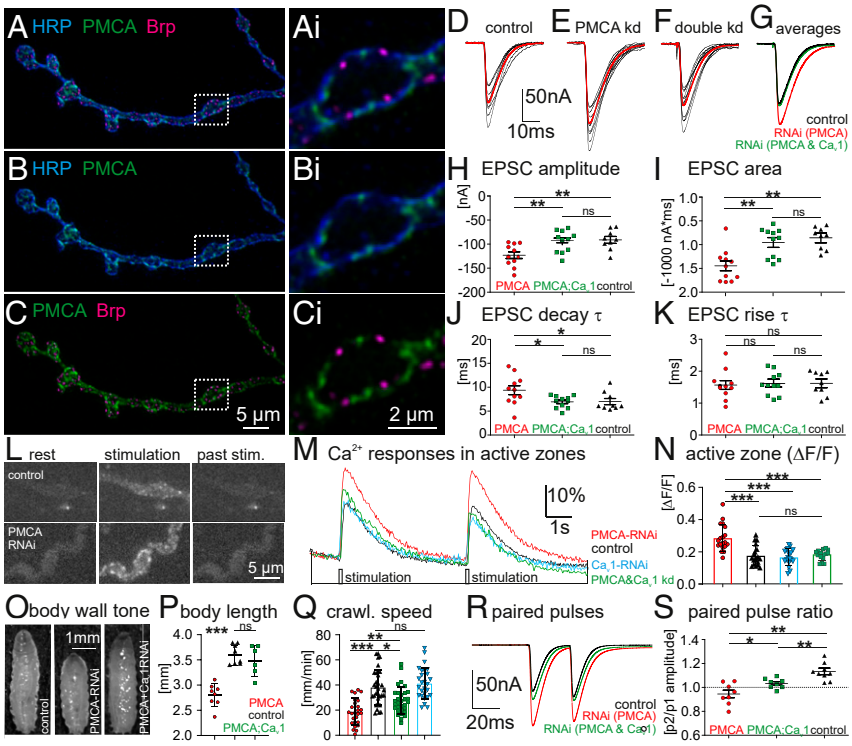

Fig. 3. PMCA separates presynaptic Ca_v1 and Ca_v2 channel function. (*A*–*C*) Representative confocal Z-projection of terminal motor axons stained for neuronal surface by α–HRP (blue), AZs with α–Brp (magenta), and Venus-tagged plasma membrane calcium ATPase PMCA (green). Dotted white box demarks area enlarged and shown as single optical sections in (*A*, *i*–*C*, *i*). (*D*–F) Evoked PSCs in 0.5 mM external Ca^{2+} from muscle M6/7 as multiple sweeps (black traces) and average (red) in a representative control (*D*), following PMCA-kd in motoneurons (*E*), and with PMCA, Ca_v1 double knockdown (*F*). (*G*) Overlay of averages shows increased amplitude in PMCA-kd (red) versus control (black) and restoration by concomitant Ca_v1-kd (green). PSC amplitude (*H*), area (*I*), and time constant of decay (*J*) are significantly increased with presynaptic PMCA-kd (red circles) compared with the control (black triangles). Effects of PMCA-kd on evoked synaptic transmission are rescued by concomitant Ca_v1-kd (green squares). (*K*) PSC rise time is not affected. (*L*–*N*) Imaging with GCaMP6s coupled to Brp reveals local AP-induced Ca^{2+} signals at presynaptic AZs before, during, and after stimulation (10 APs at 100 Hz) for control (*L*, *Upper* images) and with PMCA-kd (*L*, *Lower* images). (*M* and *N*) Quantification reveals no differences in evoked AZ Ca^{2+} signal amplitudes upon Ca_v1-kd (blue) but a nearly twofold, significant increase with PMCA-kd (red) compared with the control (black). (*O*) PMCA-kd in motoneurons increases muscle tone thus shortening body length (*P*) and is rescued by Ca_v1-kd. (*Q*) Compared with the control (black triangles), crawling speed is significantly decreased by PMCA-kd (red circles) but not affected by Ca_v1-kd (blue triangles). Ca_v1-kd in PMCA-kd (green squares) partially rescues reduced locomotion speed. (*R* and *S*) Mild paired pulse facilitation as observed in controls (black) is converted to mild paired pulse depression by PMCA-kd (red). Concomitant Ca_v1-kd yields partial rescue (green). $*P < 0.05$; $**P < 0.01$; $***P < 0.001$; ns, not significant.

way, Ca^{2+} influx through Ca_v1 and Ca_v2 channels independently control two fundamental aspects of synapse function; Ca_v2 is essential for AP-triggered SV exocytosis due to the central position within the AZ, whereas Ca_v1 augments SV recycling and modulates the dynamic coding properties of the synapse from its more peripheral location around AZs. However, we cannot rule out the possibility that Ca^{2+} influx through Ca_v2 also contributes to SV endocytosis regulation.

Functional Separation of Ca_v2 and Ca_v1 Channel at the Presynapse. Synaptic coding reliability likely requires some independence of evoked release from Ca^{2+} signals regulating endocytosis. But how do Ca^{2+} signals evoked by the same AP(s) yet mediated through Ca_v1 and Ca_v2 in adjacent subregions of the presynaptic membrane remain functionally separated? It has been demonstrated that the local Ca^{2+} signals through Ca_v2 that trigger release at AZs are confined in their spatiotemporal extent by endogenous buffers (1). The free or resting cytosolic Ca^{2+} that remains in the presynaptic terminal after nanodomain collapse through diffusion is buffered in the nanomolar range (5), but free Ca^{2+} concentrations that reportedly accelerate SV endocytosis are in the micromolar range (14, 28). Therefore, Ca_v2-triggered SV exocytosis unlikely interferes with endocytosis regulation, but it is less clear how Ca^{2+} signals for endocytosis regulation through Ca_v1 channels are prevented from interfering with release.

Next to the more distant localization of Ca_v1 channels from the AZ and cytosolic Ca^{2+} buffers (1), we considered the involvement of the plasma membrane Ca^{2+} ATPase (PMCA) as a possible means to achieve such isolation of Ca^{2+} signals. While PMCA has been found at vertebrate synapses (29, 30), it has also been shown to play a major role in Ca^{2+} homeostasis at the larval NMJ (31). However, its actual distribution within presynaptic terminals remained elusive. At the larval NMJ, strong enrichment of PMCA in the multilayered postsynaptic membrane compartment (the so-called subsynaptic reticulum [SSR]) precludes direct assessment of its presynaptic localization. We therefore employed postsynaptic PMCA-kd to uncover the precise localization of PMCA in the presynaptic membrane (*SI Appendix*, Fig. S4). PMCA exclusively localizes outside AZs (i.e., alternating with Brp puncta along the perimeter of the presynaptic terminal) (Figs. 3 *A–C*), which was substantiated by quantitative colocalization analysis (PCC for PMCA/Brp = 0.026 ± 0.019; M1 = 0.212 ± 0.014; M2 = 0.041 ± 0.033; *SI Appendix*, Fig. S4*C*).

In conditions that cause a severe but still nonlethal knockdown of PMCA (PMCA-kd) in motoneurons (*SI Appendix*, Fig. S4 *D–E*), no overt malformation of NMJs is observed. Quantitative analyses nonetheless reveal decreased AZ number and density in parallel with moderately increased postsynaptic glutamate receptor (GluR) levels (*SI Appendix*, Fig. S5). If these structural changes manifested physiologically, decreases in SV release due to lower AZ density would co-occur with increases in postsynaptic responses due to increased GluR levels and, thus at the most, cause mild changes in synaptic transmission. Presynaptic PMCA-kd, however, considerably increases the amplitude and duration of evoked PSCs (Fig. 3 *D*, *E* and *H–K*). These effects are unlikely caused by a redistribution of Ca_v1 toward AZs upon PMCA-kd, because the localization of Ca_v1 relative to Brp is similar with presynaptic PMCA-kd (PCC, 0.329 ± 0.027; M1 = 0.335 ± 0.195; M2 = 0.593 ± 0.134, n = 5) compared with the control (PCC, 0.297 ± 0.027; M1 = 0.275 ± 0.032; M2 = 0.611 ± 0.034; n =10, *SI Appendix*, Fig. S1 *C* and *D*). Both effects are dependent on Ca^{2+} influx through Ca_v1 channels, as they are reverted when PMCA and Ca_v1 are knocked down concomitantly (Fig. 3 *D–G*). To rule out that this is due to reduced strength of GAL4-driven UAS-PMCA-kd in the presence of a second UAS-transgene, we coexpressed the PMCA-kd together with UAS-GFP-RNAi. This does not reduce PSC amplitude (*SI Appendix*, Fig. S6 *A* and *B*). As an additional control, we also expressed Ca_v1-kd in a hypomorphic basigin (bsg^{SH1217}) mutant background. Fly basigin is the single ortholog of the vertebrate Ig domain proteins basigin and neuroplastin, which have been identified as binding partners essential for PMCA stability and function (29, 32, 33). Moreover, in *Drosophila*, bsg is required presynaptically to inhibit asynchronous evoked SV release (34). Our recordings not only confirm these data but also show that Ca_v1-kd partially rescues PSC amplitudes and fully rescues PSC area in bsg^{SH1217} mutants (*SI Appendix*, Fig. S6 *C–E*). Loosely coupled calcium channels have previously been considered a potential cause for increased PSC areas in bsg^{SH1217} mutants (34). In fact, both PMCA-kd and reduced PMCA function in *bsg* mutants can be rescued by Ca_v1-kd. Together, these data suggest that the low capacity, high affinity Ca^{2+} extrusion pump PMCA operates as a membrane-bound buffer that is strategically localized within the presynaptic membrane to prevent spill-over into AZs of Ca^{2+} entering through Ca_v1 channels. To further test this, we used GCaMP6s fused to Brp as an AZ-restricted Ca^{2+} sensor (35) (Fig. 3 *L* and Movie S1). Consistent with small effects of Ca_v1 on evoked synaptic transmission, Ca_v1-kd does not significantly reduce evoked Ca^{2+} signals in AZs (Fig. 3 *M* and *N*). By contrast, AZ Ca^{2+} signals are significantly increased by presynaptic PMCA-kd (Fig. 3 *M* and *N* and Movie S2), and the effect of PMCA-kd can be rescued by concomitant Ca_v1-kd (Fig. 3 *M* and *N*). This supports the conclusion that PMCA activity separates Ca_v2 signals from adjacent presynaptic Ca_v1-mediated Ca^{2+} signals, also triggered by presynaptic APs. As additional control, we estimated the resting Ca^{2+} levels in presynaptic boutons with bicistronic expression of tdTomato and GCaMP5G for ratiometric cytosolic [Ca^{2+}] measurement under UAS control (36). No significant differences were observed in tdTomato, GCaMP5G, or normalized GCaMP fluorescence intensities between control and PMCA-kd (*SI Appendix*, Fig. S6*H*). Therefore, the significant increases of PSC amplitude and area in PMCA-kd are unlikely a result of differences in resting calcium. Moreover, increased synaptic transmission as caused by PMCA-kd can be acutely rescued by bath applying the membrane permeable, slow Ca^{2+} buffer EGTA-AM (*SI Appendix*, Fig. S6 *F* and *G*), further ruling out effects of structural changes (*SI Appendix*, Fig. S5) and corroborating the impact of activity-dependent, peripheral Ca^{2+} signals onto SV release when PMCA abundance is reduced.

This constitutive function of PMCA is behaviorally relevant. PMCA-kd in motoneurons increases muscle tone such that body length of L3 larvae is reduced by ∼25% (Fig. 3 *O* and *P*), and their locomotion is significantly slower (Fig. 3 *Q*). Morphological and behavioral effects of PMCA-kd can be fully (body tone, Fig. 3 *P*) or partially rescued (locomotion, Fig. 3 *Q*) by concurrent Ca_v1-kd. Ca_v1-kd alone has no effect (Fig. 3 *Q*). Therefore, postural and locomotor defects as observed with PMCA-kd are caused by increased synaptic transmission amplitudes through functional coupling of Ca_v1 channels to SV exocytosis.

PMCA Functionally Isolates AZs and Controls SV Release Probability. The protection of readily releasable SVs by PMCA from adjacent Ca^{2+} signals also limits spontaneous release. Both the frequency and mean amplitude of spontaneously occurring PSCs recorded in TTX (10^{-6} M) are significantly increased by PMCA-kd (Fig. 4 *A–F*). Concomitant knockdown of PMCA and Ca_v1 partially rescues spontaneous release (Fig. 4 *A–F*), indicating that PMCA protects readily releasable SVs from spill-over of Ca_v1-derived and probably other Ca^{2+} signals from outside the AZ. A thorough quantal analysis of PSCs is complicated by the large sizes of M6/7 muscle fibers innervated by branched motor terminals harboring 781 ± 141 AZs. We therefore analyzed spontaneous SV release by monitoring postsynaptic Ca^{2+} influx through GluRs, using a muscle membrane–tethered GCaMP6m reporter (Fig. 4 *G–L*). Spontaneous SV release in TTX can be detected at the level of single receptor fields as unitary amplitude Ca^{2+} signal. In controls (Movie S3), frequency distribution diagrams reveal mostly single

events but lower probabilities of two- or threefold amplitudes (Fig. 4 *J*, black bars). Increases in spontaneous release upon PMCA-kd and rescue by concomitant Ca_v1-kd is also confirmed in higher external Ca^{2+} (2 mM, *SI Appendix*, Fig. S7). Integer multiples of unitary amplitudes likely reflect release from adjacent AZs, eliciting a fused Ca^{2+} signal by the sensor, which localizes to the SSR around GluR fields. Colabeling of presynaptic AZs supports this interpretation (*SI Appendix*, Fig. S8). With presynaptic PMCA-kd (Movie S4), the frequency distribution is shifted toward higher integer multiples (Fig. 4*K*). This supports the interpretation that PMCA keeps SV release probability in check. The effect of PMCA-kd is rescued by concomitant knockdown of Ca_v1 (Fig. 4 *L* and Movie S5), but Ca_v1-kd alone has no significant effect as compared to control (Fig. 4 *J*).

The functional coupling of multiple adjacent AZs upon presynaptic PMCA-kd significantly increases mean quantal content during evoked release. In controls, a presynaptic AP on average elicits calcium transients on two to three distinct postsynaptic sites underneath each presynaptic type 1b bouton (Fig. 4 *M*, closed circles; Movie S6). With 10 to 20 AZs per bouton (37), this results in an estimated release probability of 0.2, meaning that on average about 150 of the roughly 780 AZs release a single SV upon each AP. This matches the mean quantal content of 150 as estimated also by whole muscle fiber electrophysiology, thus indicating that postsynaptic Ca^{2+} imaging is a reasonable measure of release probability at single synaptic sites. Single-site release probability was clearly increased upon presynaptic PMCA-kd (Fig. 4 *N*, closed circles; Movie S7). In particular, we observed coactivation of many neighboring sites during any given stimulus, indicating that the isolation of presynaptic AZs from Ca^{2+} spill-over from their neighbors is lost. This proximity effect complicated accurate counts of active sites per stimulus. Therefore, per AP we normalized total postsynaptic fluorescence for each bouton to bouton size. PMCA-kd causes a more than twofold increase of evoked responses imaged at the level of single boutons, and this effect is rescued by concomitant knockdown of presynaptic Ca_v1 channels (Fig. 4 *O* and Movie S7). This underscores our interpretation that PMCA protects AZs from AP-triggered Ca^{2+} influx though Ca_v1, while allowing for Ca_v1-mediated augmentation of SV endocytosis outside AZs.

Discussion

Our data show strict functional separation of AP-triggered neurotransmitter release by Ca_v2 and activity-dependent modulation of SV recycling and short-term plasticity by Ca_v1 VGCCs. Although task sharing and partial redundancy among Ca_v2 isoforms is known for mammalian synapses (9, 38), and the dynamic regulation of their relative abundance within AZs can add to synaptic plasticity (39), insight into mechanisms that allow for the separate regulation of different aspects of presynaptic function by Ca_v2 and Ca_v1 channels is sparse.

Division of Labor among Presynaptic Ca_v1 and Ca_v2 Channels, Peculiarity or General Principle? Ultrastructural support for the coexistence of Ca_v2 and Ca_v1 channels has been obtained in rat hippocampal neurons, where Ca_v2 localizes to AZs and Ca_v1 outside AZs (20),

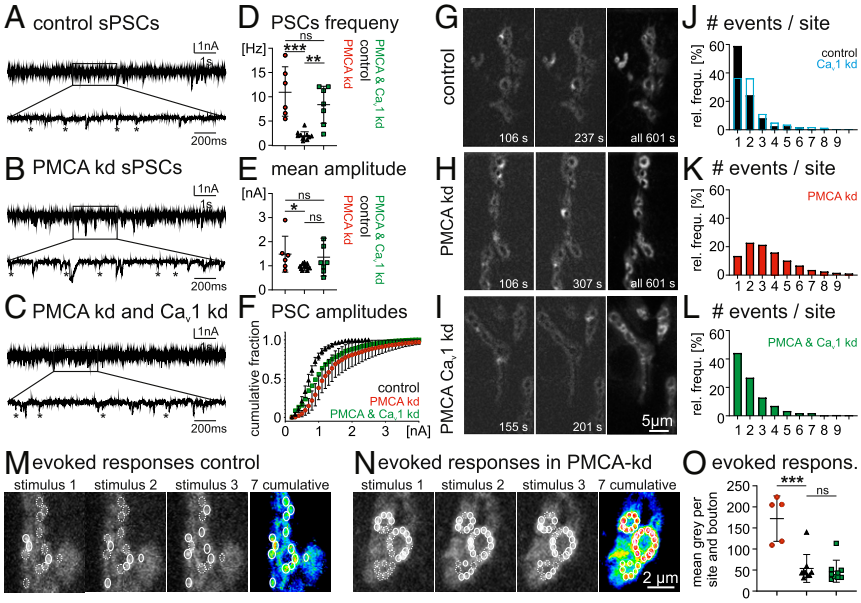

Fig. 4. PMCA confines spontaneous and evoked SV release. (*A–C*) Spontaneous PSCs (sPSCs) at the NMJ in TTX (10^{-6}) and 0.5 mM Ca^{2+} in control (*A*), with motoneuronal PMCA-kd (*B*) and with PMCA, Ca_v1 double-kd (*C*). Lower traces are at enlarged time scale. Asterisks demark smallest amplitude sPSCs, which are similar among genotypes (control, 0.6 ± 0.08 nA; PMCA kd, 0.68 ± 0.16 nA, PMCA, Ca_v1 kd, 0.64 ± 0.15 nA). (*D*) sPSC frequency is significantly increased by PMCA-kd (red) as compared to control (black) and reduced but not rescued by concomitant Ca_v1-kd (green). (*E*) Mean sPSC amplitude is increased by PMCA-kd (red) and partially rescued by concomitant Ca_v1-kd (green). *(F)* Similarly, cumulative sPSC amplitudes of controls (black) are significantly increased by PMCA-kd (red), which is partially rescued by concomitant Ca_v1-kd (green), thus confirming the analysis of mean amplitudes *(E)* on the distribution level. (*G–L*) Imaging of responses to spontaneous SV release in TTX (10^{-6} M) by postsynaptic GCaMP6m expression in control (*G*), with presynaptic PMCA-kd (*H*) and with presynaptic PMCA, Ca_v1 double-kd (*I*). Left two columns exemplify events at single time points, and the right column is a maximum projection over 601 s. (*J*) Frequency distribution of fluorescence intensities, analyzed separately for each postsynaptic site and binned to multiple integers of smallest amplitude unitary events, is dominated by unitary events in controls (black bars) and not significantly affected by Ca_v1-kd in motoneurons (blue). (*K*) Presynaptic PMCA-kd shifts the distribution to the right. (*L*) This shift is rescued by concomitant Ca_v1-kd. (*M–O*) Postsynaptic responses to AP-triggered SV release in control (*M*) and with presynaptic PMCA-kd (*N*). (*M*) In response to each AP (exemplified for 3 APs, stimuli 1 through 3), a different subset of postsynaptic sites (closed white circles) is activated, while other sites remain silent (dotted white circles). The number of activated sites per bouton is increased by presynaptic PMCA-kd, with coactivation of neighbors. False color-coded images on the right show cumulative intensity distributions for 7 APs in control (*M*) and with PMCA-kd (*N*). (*O*) Quantification of total fluorescence normalized to bouton size reveals significantly increased responses in PMCA-kd (red circles) compared with the control (black triangles), and this is rescued by concomitant Ca_v1-kd. $^*P < 0.05$; $^{**}P < 0.01$; $^{***}P < 0.001$; ns, not significant.

largely as we find for *Drosophila*. Moreover, pharmacological data in mammals indicate that Ca_v1 and Ca_v2 VGCCs separately control SV release and synaptic plasticity (40). In synapses of the amygdala, Ca_v1 is not required for SV release but for presynaptic forms of LTP (11); in GABAergic basket cells, Ca_v1 is not required for evoked release but for posttetanic potentiation (7); and at mouse neuromuscular synapses, anatomical (41) and physiological data (42) indicate the presence of both presynaptic Ca_v1 and Ca_v2 channels, but again with little contribution of Ca_v1 to evoked SV release (42). Therefore, studies of different synapse types in various species support the idea that multiple fundamental aspects of presynaptic function are executed in parallel on the basis of spatially separated VGCCs with different kinetics and conductances. This study provides a mechanism for functional separation in the small space of the axon terminal (see Figs. 3 and 4, and *Discussion*, last section).

The fast activation and inactivation kinetics of Ca_v2 channels in the AZ seem well suited for tight excitation-release coupling, and Ca_v2 activation mediates release mostly in an all or none fashion, though dynamic modulation of channel-SV coupling to adjust release probability is reported (9, 39, 43). By contrast, Ca_v1 channels typically have larger single-channel conductances and slower inactivation kinetics, suggesting that they are well suited to cope with the need for relatively high Ca^{2+} and the slow time course of endocytic vesicle retrieval.

Presynaptic Ca_v1 Channels and Endocytosis Regulation. Endocytosis regulation by activity-dependent Ca^{2+} influx is discussed for mammalian and invertebrate synapses (14). At the *Drosophila* NMJ, separate Ca^{2+} entry routes for differential exo- and endocytosis regulation have been postulated (23), and the SV-associated calcium channel Flower has been suggested to contribute to this function (44). We identify Ca_v1 channels within the periphery of AZs as a distinct entry route for Ca^{2+}-dependent augmentation of SV endocytosis. Although the precise underlying mechanisms remain to be investigated, an attractive hypothesis is that Ca_v1 may serve as an activity-dependent switch to direct recycling into different SV pools. In basket cells, Ca_v1 mediated Ca^{2+} influx has been speculated to mobilize vesicles into the releasable pool to maintain synaptic transmission during high-frequency bursting (7). Similarly, at the mouse NMJ, pharmacological blockade of L-type Ca_v1 channels decreases FM2-10 loading and quantal release upon high-frequency stimulation (45). This is in line with our findings of increased synaptic depression, reduced SV reacidification, decreased FM1-43 uptake, and reduced PSC recovery after RRP depletion upon reduction of presynaptic Ca_v1 function. However, the effects of Ca_v1-kd manifest within few seconds. Unless recycling and SV reformation are ultrafast, this seems too fast for SV reuse. In cultured hippocampal neurons, for example, SVs are not reused during the first 200 APs, irrespective of stimulation frequency between 5 and 40 Hz (27). However, given that endocytic proteins can also function in release site clearance (27), reduced endocytosis in Ca_v1-kd may increase synaptic depression and decrease recovery from RRP depletion indirectly as a result of reduced release site clearance. We can also not exclude additional effects of Ca_v1 channels on other steps in the SV cycle, such as SV priming.

For the mouse NMJ, it has been inferred that Ca_v1 activity directs recycled SVs into a high-probability release pool (45). Ultrastructural analysis of *Drosophila* synapses has also revealed two different recycling modes, one that depends on external Ca^{2+} and directs recycled SVs to AZs and another one that does not depend on external Ca^{2+} and replenishes other SV pools (46). Taken together, peri-AZ localization of presynaptic Ca_v1 channels as found in hippocampus (20) and at the *Drosophila* NMJ (this study) may provide a common control mechanism to direct SV recycling to different pools in an activity-dependent manner. Protection of AZs by the peri-AZ PMCA provides a mechanism to maintain mean quantal content, and thus coding reliability, in the face of Ca^{2+}-mediated endocytosis regulation.

As in many mammalian neurons (47), in *Drosophila* motoneurons, Ca_v1 channels localize also to dendrites to boost excitatory synaptic input (19). Therefore, cooperative functions of Ca_v1 channels in different subneuronal compartments coordinate firing and SV recycling rates. Moreover, as in spinal motoneurons (47), *Drosophila* Ca_v1 channel function is modulated by biogenic amines (21), thus providing means for integrative regulation of motoneuron excitability and SV recycling rates in the context of internal state and behavioral demands.

PMCA Controls Release Probability by AZ Protection from Ca_v1 and Is Adjustable. Here, we show that 1) axon terminal Ca_v1 segregates into the peri-AZ compartment to augment SV endocytosis, and 2) PMCA, rather than directly acting on Ca^{2+} entering through Ca_v2, actively controls Ca_v1-dependent Ca^{2+} changes, thereby enabling side-by-side Ca^{2+} domains with profiles that meet the different requirements for SV release and recycling. This is consistent with reports on spatially restricted expression and/or regulation of PMCA in small T lymphocytes as a means to steer Ca^{2+}-dependent processes specifically within cellular microdomains (32, 48). In consequence, we propose to expand the concept of controlling release probability by presynaptic Ca^{2+} buffering systems after nanodomain collapse, which has been scrutinized in many studies (1, 5), with the idea of nanodomain protection from presynaptic Ca^{2+} signals originating outside the AZ.

PMCAs have high Ca^{2+} affinity (49) and can accelerate Ca^{2+} clearance on millisecond timescales (29, 31). While isolating AZs from Ca^{2+} influx through Ca_v1, PMCA otherwise does not affect the spatiotemporal properties of AZ Ca^{2+} nanodomains, because transmission amplitudes are not altered by PMCA-kd in the absence of Ca_v1 channels (Fig. 3 *D–J*). Instead, it ensures stable release probability in the face of presynaptic Ca^{2+} signals that augment SV recycling, shape APs (50), and control synaptic plasticity. In contrast to soluble Ca^{2+} buffers and fixed ones in the AZ (1), the membrane-bound peri-AZ PMCA can be regulated on short time scales (e.g., by downstream effectors of Ca^{2+} and phospholipids) (49, 51). In addition, release from autoinhibition by binding of Ca^{2+}/calmodulin, which is conserved across phyla (52), provides a molecular memory due to the slow time course of calmodulin release, allowing PMCA to persist in a preactivated state and to respond instantaneously to the next Ca^{2+} signal (53). Therefore, PMCA-mediated control of SV release probability is likely adjusted by the local activity at the synaptic terminal. Our data show that changes in PMCA-dependent AZ protection largely impact SV release probability by allowing or preventing functional coupling of Ca_v1 channels with readily releasable SVs. We propose that the distant localization of Ca_v1 channels and PMCA in between AZs enables effective and versatile regulation of synaptic strength on a short time scale. In fact, theoretical considerations (54) and recent studies on $Ca_v2.1$ dynamic coupling in hippocampal synapses (3, 10) and on differential spacing of Ca_v2 channels in cerebellar synapses (4) suggest that modulation of SV release probability favors loose coupling of VGCCs to SV. Thus, regulation of presynaptic PMCA activity emerges as an effective means to dynamically regulate plasticity and SV recycling rates downstream of Ca_v1.

Materials and Methods

Full methods and all genotypes used are available in *SI Appendix*.

Animals. *Drosophila melanogaster* were reared at 25 °C on a 12-h light-dark cycle on standard cornmeal diet (19). Third instar larvae of both sexes were used for experiments (see *SI Appendix*, Table S1 for complete list of all genotypes used).

Electrophysiology. Single-electrode current clamp recordings and two electrode voltage clamp recordings from larval muscle fibers were conducted at 25 °C (if not noted otherwise) with thin-walled borosilicate glass microelectrodes (Sutter, BF100-50-10) filled with 3 M potassium chloride and acquired with an Axoclamp 2B amplifier, a Digidata 1320, and PClamp10 software (all Molecular Devices). All recordings were performed in HL3.1 saline containing (in mM) NaCl 70, KCl 2.5, $MgCl_2$ 2, $CaCl_2$ 0.5 or 2, $NaHCO_3$ 10, trehalose 5, sucrose 115 or 109 (when $CaCl_2$ was 2), and Hepes 5 (pH adjusted to 7.24 to 7.25 with 1 N NaOH, mOsm: 310).

Live imaging. All presynaptic calcium signals at the NMJ were acquired in the presence of 7 mM extracellular glutamate to minimize movement. AP-triggered presynaptic Ca^{2+} signals in animals expressing *UAS-GCaMP6f* under the control of *vGlut^{OK371}-GAL4* in motoneurons were imaged with an Orca Flash 4.0LT Model C11440-42U CMOS camera (Hamamatsu) mounted on a fixed stage upright Zeiss Axio Examiner A1 epifluorescence microscope and controlled with HOKAWO 3.00 software as previously described (21). For imaging of Ca^{2+} signals in presynaptic AZs, the *UAS-brp.S-mCherry-GCaMP6s* transgene (GCaMP6s and mCherry fused to the AZ protein Brp) was expressed under the control of *vGlut^{OK371}-GAL4* to localize AZs in the mCherry channel and image GCaMP6s fluorescent changes in AZs. The UAS-nSyb-pH transgene [SynaptopHluorin, (55)] was expressed in motoneurons under the control of *vGlut^{OK371}-GAL4* to assess endocytosis by imaging SV reacidification at different time intervals after RRP depletion by high-frequency motoneuron stimulation (60 Hz, 1 s). SV release and recycling were visualized by unloading and loading of the styryl dye FM1-43 (Molecular Probes T35356). Following dissection in calcium-free HL3.1 saline, a first image was taken of motoneuron boutons on M6/7 to determine resting fluorescence [F(rest)]. Next, motoneuron activity and loading of FM1-43 into recycled SVs was induced by perfusion with modified high potassium HL3.1 saline containing 0.5 mM calcium, 20 mM potassium, and 2 μM FM1-43 for 3 min. Immediately after washing for 3 min in calcium- and FM1-43-free normal HL3.1 saline, the second image was taken to determine fluorescence intensity after FM1-43 loading into recycled SVs [F(load)]. Preparations were restimulated by perfusion with 0.5 mM calcium and 20 mM potassium saline and washed for an additional 3 min in calcium-free HL3.1 saline to determine fluorescence intensity in boutons after FM1-43 unloading [F(unload)]. Background was subtracted from all images. ΔF/F was calculated as [F(load) − F(rest)]/F(rest) for loaded boutons and as [F(unload) − F(rest)]/F(rest) for unloaded boutons.

For GAL4/UAS-based transgene expression in motoneurons and simultaneous imaging of Ca^{2+} influx through postsynaptic glutamate receptors, we generated a constitutively muscle-expressed version of a previously described *UAS-myrGCaMP5* reporter (56). Images were acquired with a CSU-X1 spinning disk (Yokogawa) on an upright Olympus BX51WI microscope and an EMCCD camera (iXon+897, Andor Technology). Recordings were obtained in normal HL3.1 saline in 0.5 and 2 mM Ca^{2+}. Spontaneous events with and without 1 μM TTX were recorded at 20 Hz acquisition rate for a duration of 250 s (5,000 frames). Evoked responses were recorded without TTX and induced by motor nerve stimulation with a suction electrode. Presynaptic resting calcium levels were measured by expressing the P2A peptide to coexpress the red fluorescent protein tdTomato and the genetically encoded calcium indicator GCaMP5G in motoneurons (36) in controls and in combination with PMCA-kd. Ratiometric imaging under a silicone immersion objective lense (100×, NA 1.35) was used to compensate for alteration of fluorescent intensities at different optical planes and expression levels. Image stacks were acquired with a Digital CMOS camera (ORCA-Flash4.0; Hamamatsu) and analyzed using custom-written routines in Fiji (NIH, https://imagej.net/software/fiji/).

Immunocytochemistry. Triple immunostaining was conducted with rabbit α-GFP (1:400) for tagged Ca_v2 channels, α-Ca_v1 (goat anti-Ca_v1, 1:200), and the AZ marker bruchpilot (mouse α-Brp NC82, 1:200). For quantification of synaptic structure in different genotypes motoneuron axon terminal bouton structure was visualized with α-HRP (horse radish peroxidase, 1:500), presynaptic AZs were labeled with α-NC82 (Brp), and glutamate receptor IIc (GluRIIc) was labeled by immunocytochemistry. $PMCA^{Venus}$ signal was enhanced with an Atto488-conjugated FluoTag-X4 anti-GFP nanobody (NanoTag Biotechnologies) incubated at 1:300 for 2 h at room temperature. Histology and CLSM imaging were conducted as previously described (19).

Statistical Analysis. Significance of normally distributed datasets was examined using two-sided unpaired or paired Student's *t* tests or two-way ANOVA. For data not normally distributed, Mann–Whitney *U* test or Kruskal–Wallis ANOVA with post hoc groupwise comparison were used. Data are presented as mean ± SD or ± SEM.

Data Availability. All study data are included in the article and/or supporting information.

ACKNOWLEDGMENTS. Support by the German Research Foundation to C.D. (Du 331-6/2), to U.T. (CRC854/B08), and to M.H. and C.D. (CRC1080/B12) is gratefully acknowledged. M.H. and A.B. were supported by project support by the Schram foundation.

1. E. Eggermann, I. Bucurenciu, S. P. Goswami, P. Jonas, Nanodomain coupling between Ca^{2+} channels and sensors of exocytosis at fast mammalian synapses. *Nat. Rev. Neurosci.* **13**, 7–21 (2011).
2. Y. Nakamura *et al.*, Nanoscale distribution of presynaptic $Ca^{(2+)}$ channels and its impact on vesicular release during development. *Neuron* **85**, 145–158 (2015).
3. J. Heck *et al.*, Transient confinement of $Ca_V2.1$ Ca^{2+}-channel splice variants shapes synaptic short-term plasticity. *Neuron* **103**, 66–79.e12 (2019).
4. N. Rebola *et al.*, Distinct nanoscale calcium channel and synaptic vesicle topographies contribute to the diversity of synaptic function. *Neuron* **104**, 693–710.e9 (2019).
5. I. Delvendahl *et al.*, Reduced endogenous Ca^{2+} buffering speeds active zone Ca^{2+} signaling. *Proc. Natl. Acad. Sci. U.S.A.* **112**, E3075–E3084 (2015).
6. J. S. Dittman, T. A. Ryan, The control of release probability at nerve terminals. *Nat. Rev. Neurosci.* **20**, 177–186 (2019).
7. K. Jensen, I. Mody, L-type Ca^{2+} channel-mediated short-term plasticity of GABAergic synapses. *Nat. Neurosci.* **4**, 975–976 (2001).
8. P. E. Castillo, M. G. Weisskopf, R. A. Nicoll, The role of Ca^{2+} channels in hippocampal mossy fiber synaptic transmission and long-term potentiation. *Neuron* **12**, 261–269 (1994).
9. D. Dietrich *et al.*, Functional specialization of presynaptic Cav2.3 Ca^{2+} channels. *Neuron* **39**, 483–496 (2003).
10. N. P. Vyleta, P. Jonas, Loose coupling between Ca^{2+} channels and release sensors at a plastic hippocampal synapse. *Science* **343**, 665–670 (2014).
11. E. Fourcaudot *et al.*, L-type voltage-dependent $Ca^{(2+)}$ channels mediate expression of presynaptic LTP in amygdala. *Nat. Neurosci.* **12**, 1093–1095 (2009).
12. M. Umemiya, A. J. Berger, Single-channel properties of four calcium channel types in rat motoneurons. *J. Neurosci.* **15**, 2218–2224 (1995).
13. N. L. Kononenko, V. Haucke, Molecular mechanisms of presynaptic membrane retrieval and synaptic vesicle reformation. *Neuron* **85**, 484–496 (2015).
14. J. Leitz, E. T. Kavalali, Ca^{2+} Dependence of synaptic vesicle endocytosis. *Neuroscientist* **22**, 464–476 (2016).
15. T. Maritzen, V. Haucke, Coupling of exocytosis and endocytosis at the presynaptic active zone. *Neurosci. Res.* **127**, 45–52 (2018).
16. H. L. Atwood, S. Karunanithi, Diversification of synaptic strength: Presynaptic elements. *Nat. Rev. Neurosci.* **3**, 497–516 (2002).
17. R. J. Kittel *et al.*, Bruchpilot promotes active zone assembly, Ca^{2+} channel clustering, and vesicle release. *Science* **312**, 1051–1054 (2006).
18. K. P. Harris, J. T. Littleton, Transmission, Development, and Plasticity of Synapses. *Genetics* **201**, 345–375 (2015).
19. D. Kadas *et al.*, Dendritic and axonal L-type calcium channels cooperate to enhance motoneuron firing output during *Drosophila* larval locomotion. *J. Neurosci.* **37**, 10971–10982 (2017).
20. A. L. Tippens *et al.*, Ultrastructural evidence for pre- and postsynaptic localization of Cav1.2 L-type Ca^{2+} channels in the rat hippocampus. *J. Comp. Neurol.* **506**, 569–583 (2008).
21. N. Schützler *et al.*, Tyramine action on motoneuron excitability and adaptable tyramine/octopamine ratios adjust *Drosophila* locomotion to nutritional state. *Proc. Natl. Acad. Sci. U.S.A.* **116**, 3805–3810 (2019).
22. G. E. Rieckhof, M. Yoshihara, Z. Guan, J. T. Littleton, Presynaptic N-type calcium channels regulate synaptic growth. *J. Biol. Chem.* **278**, 41099–41108 (2003).
23. H. Kuromi, A. Honda, Y. Kidokoro, Ca^{2+} influx through distinct routes controls exocytosis and endocytosis at *Drosophila* presynaptic terminals. *Neuron* **41**, 101–111 (2004).
24. V. Haucke, E. Neher, S. J. Sigrist, Protein scaffolds in the coupling of synaptic exocytosis and endocytosis. *Nat. Rev. Neurosci.* **12**, 127–138 (2011).
25. E. Macia *et al.*, Dynasore, a cell-permeable inhibitor of dynamin. *Dev. Cell* **10**, 839–850 (2006).
26. C. Wentzel, I. Delvendahl, S. Sydlik, O. Georgiev, M. Müller, Dysbindin links presynaptic proteasome function to homeostatic recruitment of low release probability vesicles. *Nat. Commun.* **9**, 267 (2018).
27. Y. Hua *et al.*, Blocking endocytosis enhances short-term synaptic depression under conditions of normal availability of vesicles. *Neuron* **80**, 343–349 (2013).
28. P. Thomas, A. K. Lee, J. G. Wong, W. Almers, A triggered mechanism retrieves membrane in seconds after $Ca^{(2+)}$-stimulated exocytosis in single pituitary cells. *J. Cell Biol.* **124**, 667–675 (1994).
29. N. Schmidt *et al.*, Neuroplastin and basigin are essential auxiliary subunits of plasma membrane Ca^{2+}-ATPases and key regulators of Ca^{2+} clearance. *Neuron* **96**, 827–838.e9 (2017).
30. T. P. Jensen, A. G. Filoteo, T. Knopfel, R. M. Empson, Presynaptic plasma membrane Ca^{2+} ATPase isoform 2a regulates excitatory synaptic transmission in rat hippocampal CA3. *J. Physiol.* **579**, 85–99 (2007).
31. G. A. Lnenicka, J. Grizzaffi, B. Lee, N. Rumpal, Ca^{2+} dynamics along identified synaptic terminals in *Drosophila* larvae. *J. Neurosci.* **26**, 12283–12293 (2006).

32. M. Korthals *et al*., A complex of neuroplastin and plasma membrane Ca^{2+} ATPase controls T cell activation. *Sci. Rep.* **7**, 8358 (2017).
33. D. Gong *et al*., Structure of the human plasma membrane Ca^{2+}-ATPase 1 in complex with its obligatory subunit neuroplastin. *Nat. Commun.* **9**, 3623 (2018).
34. F. Besse *et al*., The Ig cell adhesion molecule Basigin controls compartmentalization and vesicle release at *Drosophila* melanogaster synapses. *J. Cell Biol.* **177**, 843–855 (2007).
35. B. Kiragasi, J. Wondolowski, Y. Li, D. K. Dickman, A presynaptic glutamate receptor subunit confers robustness to neurotransmission and homeostatic potentiation. *Cell Rep.* **19**, 2694–2706 (2017).
36. R. W. Daniels, A. J. Rossano, G. T. Macleod, B. Ganetzky, Expression of multiple transgenes from a single construct using viral 2A peptides in *Drosophila*. *PLoS One* **9**, e100637 (2014).
37. M. M. Paul *et al*., Bruchpilot and Synaptotagmin collaborate to drive rapid glutamate release and active zone differentiation. *Front. Cell. Neurosci.* **9**, 29 (2015).
38. L. Li, J. Bischofberger, P. Jonas, Differential gating and recruitment of P/Q-, N-, and R-type Ca^{2+} channels in hippocampal mossy fiber boutons. *J. Neurosci.* **27**, 13420–13429 (2007).
39. M. S. Ahmed, S. A. Siegelbaum, Recruitment of N-Type $Ca^{(2+)}$ channels during LTP enhances low release efficacy of hippocampal CA1 perforant path synapses. *Neuron* **63**, 372–385 (2009).
40. J. Subramanian, A. Morozov, Erk1/2 inhibit synaptic vesicle exocytosis through L-type calcium channels. *J. Neurosci.* **31**, 4755–4764 (2011).
41. R. Pagani *et al*., Differential expression of α 1 and β subunits of voltage dependent Ca^{2+} channel at the neuromuscular junction of normal and P/Q Ca^{2+} channel knockout mouse. *Neuroscience* **123**, 75–85 (2004).
42. F. J. Urbano, O. D. Uchitel, L-type calcium channels unmasked by cell-permeant Ca^{2+} buffer at mouse motor nerve terminals. *Pflugers Arch.* **437**, 523–528 (1999).
43. M. A. Böhme *et al*., Active zone scaffolds differentially accumulate Unc13 isoforms to tune $Ca^{(2+)}$ channel-vesicle coupling. *Nat. Neurosci.* **19**, 1311–1320 (2016).
44. C. K. Yao *et al*., A synaptic vesicle-associated Ca^{2+} channel promotes endocytosis and couples exocytosis to endocytosis. *Cell* **138**, 947–960 (2009).
45. P. P. Perissinotti, B. Giugovaz Tropper, O. D. Uchitel, L-type calcium channels are involved in fast endocytosis at the mouse neuromuscular junction. *Eur. J. Neurosci.* **27**, 1333–1344 (2008).
46. J. H. Koenig, K. Ikeda, Synaptic vesicles have two distinct recycling pathways. *J. Cell Biol.* **135**, 797–808 (1996).
47. C. J. Heckman, R. H. Lee, R. M. Brownstone, Hyperexcitable dendrites in motoneurons and their neuromodulatory control during motor behavior. *Trends Neurosci.* **26**, 688–695 (2003).
48. A. Quintana *et al*., Calcium microdomains at the immunological synapse: How ORAI channels, mitochondria and calcium pumps generate local calcium signals for efficient T-cell activation. *EMBO J.* **30**, 3895–3912 (2011).
49. E. E. Strehler, A. G. Filoteo, J. T. Penniston, A. J. Caride, Plasma-membrane $Ca^{(2+)}$ pumps: Structural diversity as the basis for functional versatility. *Biochem. Soc. Trans.* **35**, 919–922 (2007).
50. D. Kadas, S. Ryglewski, C. Duch, Transient BK outward current enhances motoneurone firing rates during *Drosophila* larval locomotion. *J. Physiol.* **593**, 4871–4888 (2015).
51. R. Lopreiato, M. Giacomello, E. Carafoli, The plasma membrane calcium pump: New ways to look at an old enzyme. *J. Biol. Chem.* **289**, 10261–10268 (2014).
52. H. Tidow *et al*., A bimodular mechanism of calcium control in eukaryotes. *Nature* **491**, 468–472 (2012).
53. A. J. Caride *et al*., The plasma membrane calcium pump displays memory of past calcium spikes. Differences between isoforms 2b and 4b. *J. Biol. Chem.* **276**, 39797–39804 (2001).
54. V. Matveev, R. Bertram, A. Sherman, Calcium cooperativity of exocytosis as a measure of Ca^{2}+ channel domain overlap. *Brain Res.* **1398**, 126–138 (2011).
55. K. E. Poskanzer, K. W. Marek, S. T. Sweeney, G. W. Davis, Synaptotagmin I is necessary for compensatory synaptic vesicle endocytosis *in vivo*. *Nature* **426**, 559–563 (2003).
56. J. E. Melom, Y. Akbergenova, J. P. Gavornik, J. T. Littleton, Spontaneous and evoked release are independently regulated at individual active zones. *J. Neurosci.* **33**, 17253–17263 (2013).